Protein Science (1999), *8*:343–354. Cambridge University Press. Printed in the USA.

Topology and dynamics of the 10 kDa C-terminal domain of DnaK in solution

ERIC B. BERTELSEN,[1] HONGJUN ZHOU,[2] DAVID F. LOWRY,[3] GREGORY C. FLYNN,[1] AND FREDERICK W. DAHLQUIST[1]

[1]Institute of Molecular Biology, University of Oregon, Eugene, Oregon 97403
[2]Macromolecular NMR Section, ABL-Basic Research Program, NCI-Frederick Cancer Research and Development Center, Frederick, Maryland 21702
[3]Environmental Molecular Sciences Laboratory, Pacific Northwest National Laboratory, 902 Battelle Boulevard, Richland, Washington 99352

(RECEIVED July 20, 1998; ACCEPTED October 19, 1998)

Abstract

Hsp70 molecular chaperones contain three distinct structural domains, a 44 kDa N-terminal ATPase domain, a 17 kDa peptide-binding domain, and a 10 kDa C-terminal domain. The ATPase and peptide binding domains are conserved in sequence and are functionally well characterized. The function of the 10 kDa variable C-terminal domain is less well understood. We have characterized the secondary structure and dynamics of the C-terminal domain from the *Escherichia coli* Hsp70, DnaK, in solution by high-resolution NMR. The domain was shown to be comprised of a rigid structure consisting of four helices and a flexible C-terminal subdomain of approximately 33 amino acids. The mobility of the flexible region is maintained in the context of the full-length protein and does not appear to be modulated by the nucleotide state. The flexibility of this region appears to be a conserved feature of Hsp70 architecture and may have important functional implications. We also developed a method to analyze ^{15}N nuclear spin relaxation data, which allows us to extract amide bond vector directions relative to a unique diffusion axis. The extracted angles and rotational correlation times indicate that the helices form an elongated, bundle-like structure in solution.

Keywords: DnaK; molecular chaperone; NMR; ^{15}N relaxation

Molecular chaperones of the Hsp70 class are expressed in response to a wide variety of cellular stresses, and are involved in a number of cellular processes under both stress and nonstress conditions. These functions include protein translocation, assembly and disassembly of multiprotein complexes, and degradation (Gething & Sambrook, 1992; Georgopoulos et al., 1994; Stuart et al., 1994). In addition, Hsp70s are thought to cooperate with members of the Hsp60 and Hsp10 classes of molecular chaperones to promote and regulate protein folding in vivo (Hendrick & Hartl, 1995). The chaperone activity of Hsp70s stems from their ability to bind and release unfolded, aggregation-prone proteins in a highly regulated manner (Rüdiger et al., 1997).

DnaK, the major *Escherichia coli* Hsp70 family member, is required for bacteriophage lambda replication and is essential for bacterial growth at most temperatures (Bukau & Walker, 1990; Georgopoulos et al., 1994). Binding and release of unfolded proteins or peptides by DnaK and other Hsp70s are tightly regulated by the cycle of ATP hydrolysis (Rüdiger et al., 1997). In the ATP bound state, the exchange of model peptide substrates is relatively fast. Hydrolysis of ATP to ADP leads to a dramatic decrease in this exchange rate. Peptide release and rebinding are then facilitated by exchange of ADP for ATP. The intrinsic rate of ATP hydrolysis in DnaK is relatively slow (turnover of $\sim$0.02 min^{-1}) (Russell et al., 1998), but can be accelerated by interactions with the protein cofactors DnaJ and GrpE. These cofactors regulate different stages of the ATPase cycle: DnaJ accelerates the hydrolysis of ATP, whereas GrpE stimulates nucleotide exchange. Together, DnaJ and GrpE can stimulate the ATPase activity of DnaK up to 50-fold (Liberek et al., 1991). Numerous DnaJ homologs and a mitochondrial GrpE homolog have been found in eukaryotic systems, suggesting a conserved mechanism of regulation of Hsp70 chaperone function (Caplan et al., 1993; Silver & Way, 1993; Bolliger et al., 1994).

Protease digestion patterns and functional analyses suggest that all Hsp70s share the same basic domain structure (Fig. 1) (Chappell et al., 1987; Kassenbrock & Kelly, 1989; Wang et al., 1993; Ha & McKay, 1994; Buchberger et al., 1995). A highly conserved 44 kDa N-terminal domain (residues 1 to 385 in DnaK) contains

Reprint requests to: Frederick W. Dahlquist, Institute of Molecular Biology, University of Oregon, Eugene, Oregon 97403; e-mail: fwd@nmr.uoregon.edu.

Abbreviations: 2D, two-dimensional; 3D, three-dimensional; CD, circular dichroism; DSS, sodium 2,2-dimethyl-2-silapentane-5-sulfonate; HPLC, high performance liquid chromatography; HSMQC, heteronuclear single multiple quantum coherence; NOE, nuclear Overhauser effect; NOESY, NOE spectroscopy; PCR, polymerase chain reaction; RMSD, root-mean-square deviation.

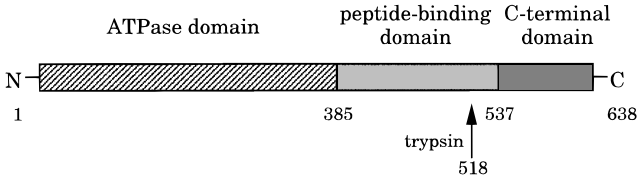

Fig. 1. Diagram of the general Hsp70 domain structure. The numbering scheme is given for DnaK. The boundary between the peptide-binding domain and the C-terminal domain is based on the crystal structure (Zhu et al., 1996). The arrow represents the trypsin cleavage site giving rise to the C-terminal fragment ($DnaK_{518–638}$) used in this study.

the ATP binding site. The peptide binding domain (residues 386 to 541 in DnaK) is ~17 kDa in size and is located immediately adjacent to the ATPase domain. Whereas the structures of both of these domains in isolation have been solved (Flaherty et al., 1990; Morshauser et al., 1995; Zhu et al., 1996; Harrison et al., 1997; Wang et al., 1998), the mechanism of coupling of the ATPase activity to peptide binding and release remains unknown. The C-terminal 10 kDa region (approximately residues 542 to 638 in DnaK) is less well conserved, and its function is unclear. The C-terminal region has often been considered a part of the peptide binding domain. However, the observation that this region is not necessary for peptide binding (Wang et al., 1993) suggested an independent function for this region. The sequence divergence in this region led to the proposal of a regulatory function, perhaps in providing specificity for interactions with cofactors or in modulation of the ATPase or peptide binding activities (Tsai & Wang, 1994).

Several studies have provided clues to the function of the C-terminal region. Tsai and Wang (1994) concluded that the C-terminal region is essential for clathrin uncoating activity in rat Hsc70, even though the ATPase and peptide binding activities seem to be unaffected by deletion of this domain. On the other hand, studies by Freeman et al. (1995) found that mutation or deletion of the C-terminal four residues of human Hsp70 affected both the ATPase and peptide binding activities. In addition, these mutations appear to alter the interaction of Hsp70 with the human DnaJ homolog, HDJ-1. This result is consistent with the observation that deletion of the C-terminal region in DnaK weakens its interaction with DnaJ (Wawrzynow & Zylicz, 1995). ATP-induced conformational changes in DnaK, however, appear to be largely unaffected by deletion of the C-terminal region (Buchberger et al., 1995).

The crystal structure of a 27 kDa fragment of DnaK containing the peptide binding domain and most of the C-terminal region has been solved (Zhu et al., 1996). In this structure, the C-terminal region is described as a helical domain positioned over the peptide binding pocket. With the C-terminal domain in this position, bound peptide appears to be blocked from exchange. In an alternate crystal form, the C-terminal domain is slightly rotated away from the peptide binding site. The authors proposed a model for the regulation of peptide binding and release by the C-terminal domain in which the helix bridging the peptide binding pocket melts out in the ATP-bound form. This disruption would allow the C-terminal domain to move away from the peptide binding site, leading to an increased peptide exchange rate.

In summary, the C-terminal region appears to be an important regulatory region, although its precise role in Hsp70 function is unclear. To determine whether the C-terminal region is an independent structural domain, and as a first step in understanding how the C-terminal domain might regulate Hsp70 function, we have begun NMR analyses of the structure and dynamics of the C-terminal domain (residues 518–638). We report here that the isolated C-terminal domain is stable and adopts a mostly helical structure in solution. In addition, the last 33 amino acids constitute a highly flexible subdomain of the molecule. This flexible region appears to be a conserved feature of Hsp70 architecture, and may be important to the regulatory function of the C-terminal domain. In the process of analyzing the ^{15}N relaxation data, we developed a method to obtain the amide bond vector directions relative to a unique, symmetrical diffusion axis from data collected at several field strengths. These angles, extracted without the use of the crystal coordinates, are in good agreement with the crystal structure, suggesting this method may have general applications.

Results

Trypsin digestion

$DnaK_{518–638}$ was identified as a protease-resistant fragment in trypsin digests (Fig. 1). Specifically, a C-terminal fragment of DnaK (residues 386–638) containing the peptide binding domain and the C-terminal region was found to be resistant to digestion by trypsin (not shown). This result agrees with that of Buchberger et al. (1994), who found that a similar fragment of DnaK ($DnaK_{385–638}$) is protease resistant relative to the full-length protein, and is also consistent with the prediction that this fragment represents the conformation of the peptide binding domain in the ADP-bound state of the full-length protein (Buchberger et al., 1995; Zhu et al., 1996). On the other hand, we found that a fragment truncated within the peptide binding domain ($DnaK_{401–638}$) is rapidly processed to a 10 kDa fragment that is resistant to further proteolysis. The peptide binding domain of $DnaK_{401–638}$ does not appear to achieve a stable fold and binds peptides at least two orders of magnitude more weakly than either full-length DnaK or $DnaK_{385–638}$ (data not shown). N-terminal amino acid sequencing and mass spectrometry revealed that the protease resistant fragment begins at residue D518 and ends at residue K638, the normal C-terminus of the full-length protein. The trypsin cleavage site in this context is identical to a nucleotide-sensitive trypsin site observed in digests of full-length DnaK (Buchberger et al., 1995). Characterization by CD indicates a mostly helical domain with a melting temperature of approximately 65 °C (data not shown). Therefore, the C-terminal region of DnaK appears to be a stable, independent domain of the molecule.

Sequential resonance assignments

The ^{1}H, ^{15}N correlation spectrum of $DnaK_{518–638}$ is shown in Figure 2. Sequential backbone resonance assignments were obtained primarily through analysis of the connectivities observed in the HNCACB, and CBCA(CO)NH experiments, and from sequential NOEs provided by the 3D ^{1}H, ^{15}N NOESY-HSMQC. Data from the 3D C(CO)NH and H(CCO)NH, which provide information about amino acid type, were used to resolve ambiguity in cases where there was significant chemical shift degeneracy in the C_α and C_β resonances. This approach resulted in nearly complete assignments for the backbone N, NH, and C_α, and C_β resonances.

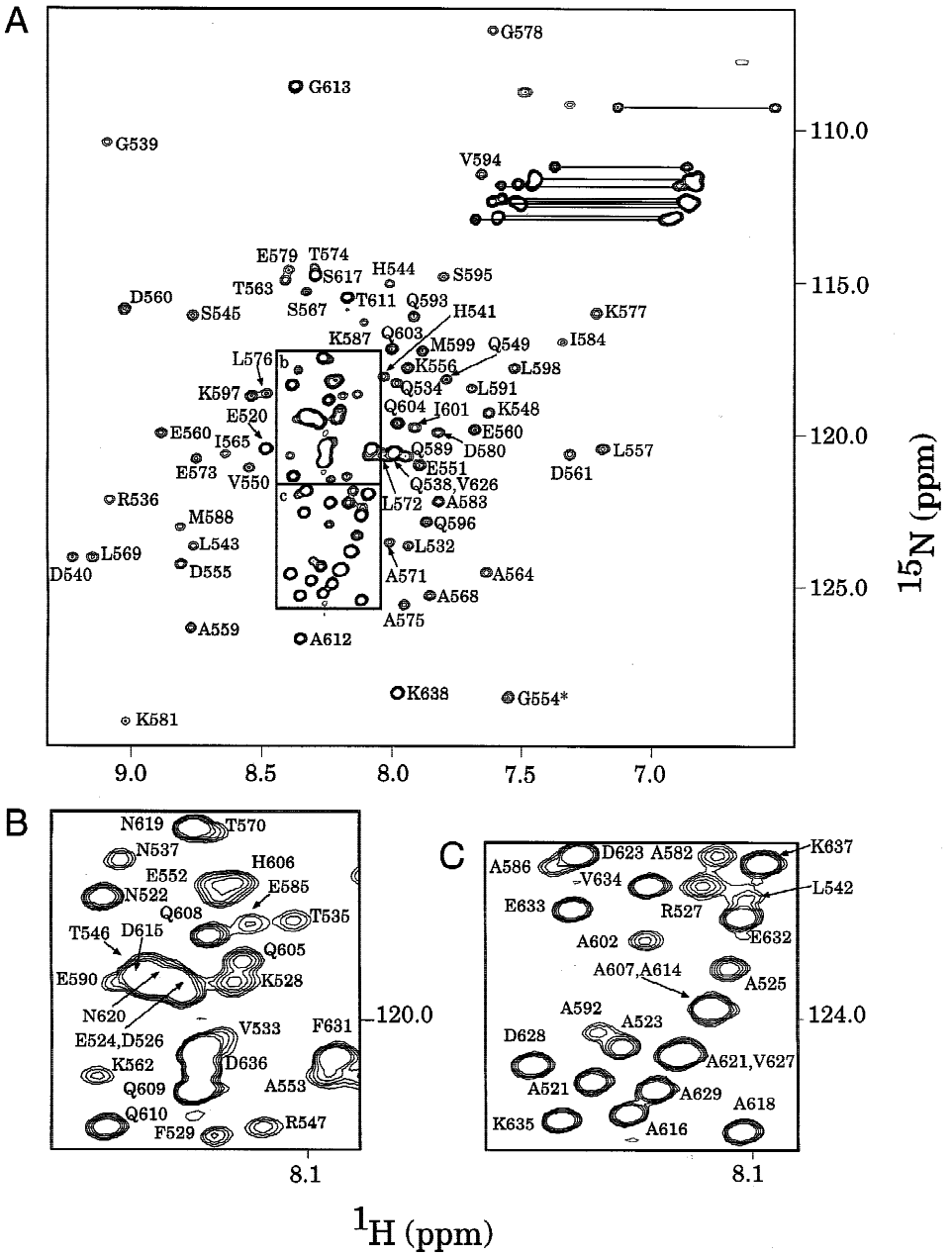

Fig. 2. ^{13}C-decoupled ^{1}H, ^{15}N correlation spectrum of uniformly ^{15}N/^{13}C-labeled DnaK$_{518–638}$. The spectrum was collected at 600 MHz and 25 °C. The protein concentration is approximately 1 mM in 50 mM sodium phosphate, 100 mM NaCl, pH 6.1. Backbone assignments are labeled according to the residue positions in full-length DnaK. The resonance from residue G554 (asterisk) is aliased in the ^{15}N dimension.

Residues 518, 530, 531, 622, 624, and 625 were not identified in the ^{1}H, ^{15}N correlation spectrum due to spectral overlap or to line-broadening caused by conformational exchange.

Secondary structure

Figure 3 contains a summary of the data used to determine the secondary structure. We found relatively few unambiguous medium range NOEs due to spectral overlap in the backbone amide and alpha protons. Because of this overlap, the secondary structure determination relies more heavily upon the chemical shift index (Wishart & Sykes, 1994), $^{3}J_{HN\alpha}$ coupling constants, and patterns of sequential NOEs. The domain consists of four helices spanning residues 532–553, 559–576, 581–593, and 596–605. Loops connect helix 1 to helix 2 and helix 2 to helix 3, but there is only a two-residue disruption in the helical structure between helix 3 and helix 4.

Two distinct classes of peaks can be distinguished in the ^{1}H, ^{15}N correlation spectrum (Fig. 2); a set of lower amplitude, broader peaks that are from the structured region (filled peak centers) and a set of intense, narrow peaks (open peak centers).

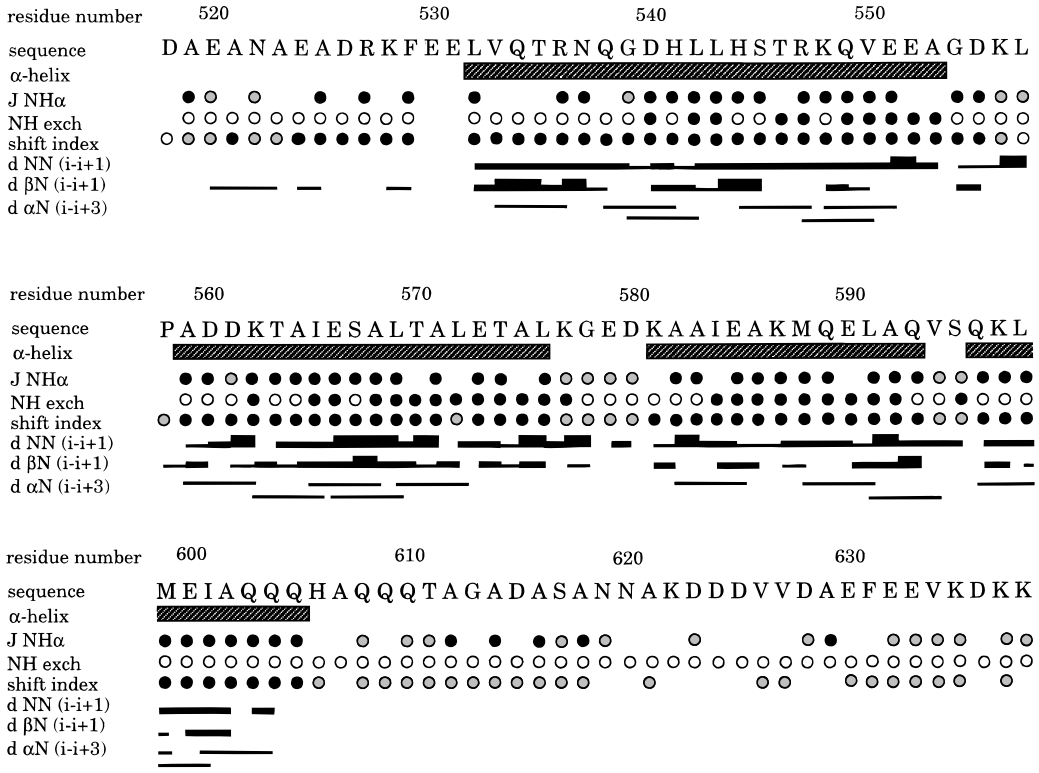

Fig. 3. Amino acid sequence and secondary structure determination. The striped bars represent α-helical segments determined by this analysis. Residues protected from hydrogen exchange by a factor of $>10^3$ relative to random coil values are depicted by closed circles. The chemical shift index represents the consensus for the C_α, C_β, and carbonyl carbon indices. Residues with α-helix, coil, or β-sheet values for the C_α chemical shift index are depicted by solid, shaded, and open circles, respectively. The shift index is omitted for residues in which the consensus could not be determined due to one or more missing assignments. $^3J_{HN\alpha}$ coupling constants are represented by solid circles for values less than 6 Hz, shaded circles for values between 6 and 8 Hz, and open circles for values greater than 8 Hz. Sequential and medium-range NOEs are represented by lines between the participating residues. The thickness of each line represents the relative intensity of the observed crosspeak.

The intense resonances were assigned to the amino-terminal approximately 15 residues and the carboxy-terminal 33 amino acids of $DnaK_{518–638.}$ The intensity and lack of chemical shift dispersion in the proton dimension for these peaks indicate a random coil conformation for these residues. However, the chemical shift index and $^3J_{HN\alpha}$ coupling constants suggest some helical structure for residues 524–529 in the amino-terminal region (Fig. 3). There are also a few intra- and inter-residual NOEs apparent for these amino acids. This region is helical in the crystal structure and makes interdomain contacts to the peptide binding domain (Zhu et al., 1996). The helical propensity of this region is therefore evident in the C-terminal domain fragment even in the absence of stabilizing contacts to the peptide binding domain. In contrast to the amino terminal region, the chemical shift index and $^3J_{HN\alpha}$ coupling constants support a random coil conformation for the 33 amino acid C-terminal "tail" region. This region is not observed in the crystal structure.

Stable helical structure, as indicated by the presence of strong sequential NOEs, appears to begin at the first residue (L532) observed to contribute core packing interactions to the helical domain in the crystal structure (Zhu et al., 1996). The high degree of protection from hydrogen exchange in helices 1, 2, and 3 indicates that the core is well packed and supports the conclusion that the isolated fragment is a stable, independent domain of the protein.

Backbone dynamics

To further characterize the dynamic behavior of $DnaK_{518–638}$, we measured backbone amide ^{15}N relaxation parameters T_1, T_2, and $^{15}N\{^1H\}$ NOE. Although the T_1 and T_2 values are roughly uniform in the helical regions, there are large differences between the helical regions and the turn regions. These differences do not seem to come entirely from increased mobilities in the turns. This together with the relatively short T_2 values for a roughly 10 kDa protein suggests that a large degree of anisotropic motion may be present. To reveal this effect and to obtain reliable values for internal motion parameters, we collected ^{15}N relaxation data at three field strengths and analyzed the data using several models.

Analysis of the dynamics data assuming isotropic tumbling yielded a poor fit of T_1/T_2 values for residues 533–603, giving τ_m approximately 10.2 ns and an average error of the fit of 44% ($\{E_1/N\}^{1/2}$, where N is the number of residues included in the fit). The fit was greatly improved when the same set of data were analyzed using the axially symmetric anisotropic model (Equation 2), yielding an average error of 8.2%. The rotational correlation times about the symmetry axis and the perpendicular axis, $\tau_\parallel$ and $\tau_\perp$, are approximately 4.8 ± 0.5 ns and 13.4 ± 0.7 ns, respectively. No significant improvement was gained in the fit by using the general anisotropic model.

The large ratio of $D_\perp$:$D_\parallel$ and the 25-fold reduction in E_1 (Equation 3) when the anisotropic model was used instead of the isotropic model indicate that the molecule undergoes significant anisotropic rotational diffusion, which is likely caused by a highly elongated shape of the molecule. The fit of the T_1/T_2 ratios using the axially symmetric diffusion model (Equation 3) also yielded the angles (α) between the amide bond vectors and the symmetric rotational diffusion axis (Fig. 4). These angles are similar for the residues in the first three helices and are mostly in the 20–35° range, but large differences are seen between these residues and those in the turns and the last helix. These results indicate that the rigid regions of the molecule form a helix bundle-like structure in solution, with the helical axes nearly parallel or antiparallel to each other, and that the last helix points slightly away from the helix bundle.

The relative amide-bond vector orientations obtained from the dynamics data were compared with those estimated from the known crystal structure (Figs. 4, 5). The crystal structure of $DnaK_{518–638}$ shows a molecule with an elongated shape, with the symmetry axis roughly pointing along the helical axes. We performed a grid search to obtain a unique, symmetric rotational axis, which best fit the set of angles α extracted from the dynamics data. This axis points roughly along the helix bundle axis. The C-terminal helix bends around residues 593–595, forming an angle of approximately 50° with the N-terminal helix bundle. The pairwise RMSD between the two sets of angles α is approximately 7.5° (Fig. 4). This consistency between the crystal structure and rotational diffusion in solution suggests that the structure in solution is similar to the crystal structure, and demonstrates that ^{15}N relaxation data can provide useful global structural information.

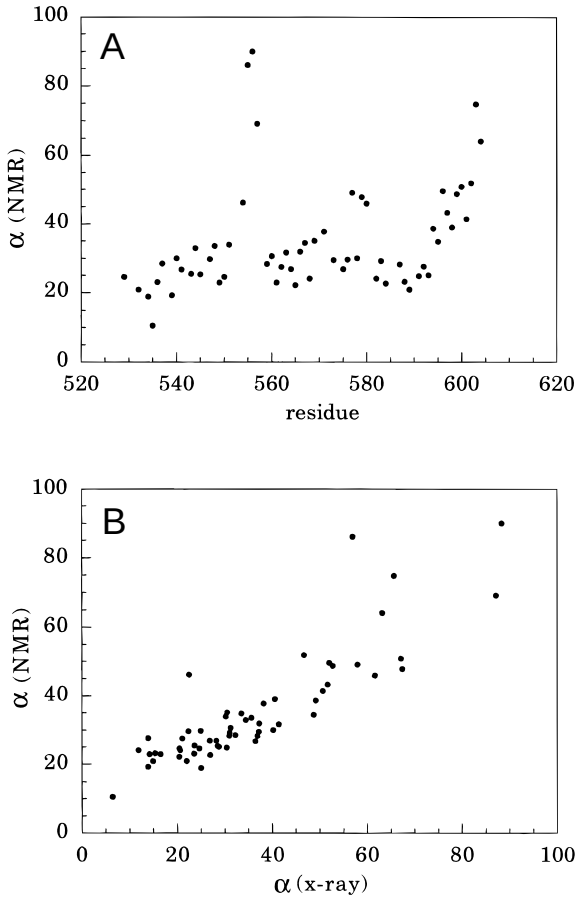

Fig. 4. Correlation of the angle α from the dynamics data with the crystal structure. The angle α was converted from $\sin^2(\alpha)$ and was folded into the 0–90° range; that is, an $(180 - \alpha)$ angle is indistinguishable from α by this method of analysis. **A:** The angle α obtained from fitting the (T_1/T_2) values (Equation 3) for each residue. **B:** The NMR-derived angle α obtained plotted against the corresponding angle from the crystal structure with the symmetrical diffusion axis as defined in Figure 5.

Values for the parameters τ_e and S^2, which describe internal motions for each residue, were extracted using the axially symmetric diffusion model, Equations 4 and 5 (Fig. 6). The structure of residues 532–604 is rigid based on the rather high values for S^2 (>0.85) for most residues. Interestingly, S^2 values are slightly lower and τ_e values are slightly higher than average in the fourth helix, suggesting a higher degree of internal motion in this region. The disruption of continuous helical structure between the third and fourth helices is accompanied by a small drop in S^2 around residues 593–594. These results, combined with reduced protection from hydrogen exchange, suggest that the fourth helix may be unstable relative to other helices. This helix packs on one side against the turn region formed by residues 554–557, which also show a relatively high degree of flexibility as evidenced by decreased S^2. The other turn region, residues 577–580, only exhibits slightly reduced S^2 relative to the helical regions.

In contrast to the apparent rigidity of residues 532–604, the N-terminus and the C-terminal 33 amino acids are highly mobile with substantially long T_2 values. These regions also show significantly reduced or negative ^{15}N{^{1}H} NOEs, and correlate well with those residues that have random coil chemical shift indices and medium $^3J_{HN\alpha}$ coupling constants (approximately 6–7 Hz). The T_1/T_2 ratios correspond to an effective correlation time of 4 to 6 ns for the N-terminal region, and 2 to 3 ns for the C-terminal region. The order parameter is around 0.6. However, for a highly flexible region, a model that assumes a single correlation time or separable overall and internal motions cannot be safely used to describe the complicated dynamics, and the meaning of an order parameter is not clear. The spectral density analysis (Fig. 6) provides a more reliable description of the dynamics although it does not provide a clear physical picture of the dynamic process. If we assume that $J(\omega)$ contains all modes of motions and can be described by $J(\omega) = \Sigma_i\, a_i\, \tau_i/[1 + (\omega\tau_i)^2]$ (Lipari & Szabo, 1982), $J(0) = \Sigma_i\, a_i\, \tau_i$ can then be considered as a weighted, average correlation time of all modes of motions, and $J(\omega_N)$ and $J(\omega_H)$ are the contributions of motions on a time scale of $1/\omega_N$ and $1/\omega_H$, respectively. The $J(0)$ values are mostly between 8 and 13 ns for residues 532–604, and mostly within 0.5 to 2 ns for the C-terminal region. The N-terminal region has slightly larger $J(0)$ values (2 to 5 ns) than the C-terminal region, supporting the view that there is some residual structure in this region. The drop in $J(0)$ in the flexible regions relative to the structured region is accompanied by an increase in $J(\omega_H)$ and $J(\omega_N)$, with $J(\omega_H)$ increased by a factor of 4. These results indicate that the motions in the N- and C-terminal regions are shifted significantly toward high-frequency modes, indicative of high flexibility across a wide dynamic range from ps to ns.

Characterization of full-length DnaK

We considered the possibility that the C-terminal mobile region is involved in interdomain contacts in the context of the full-length

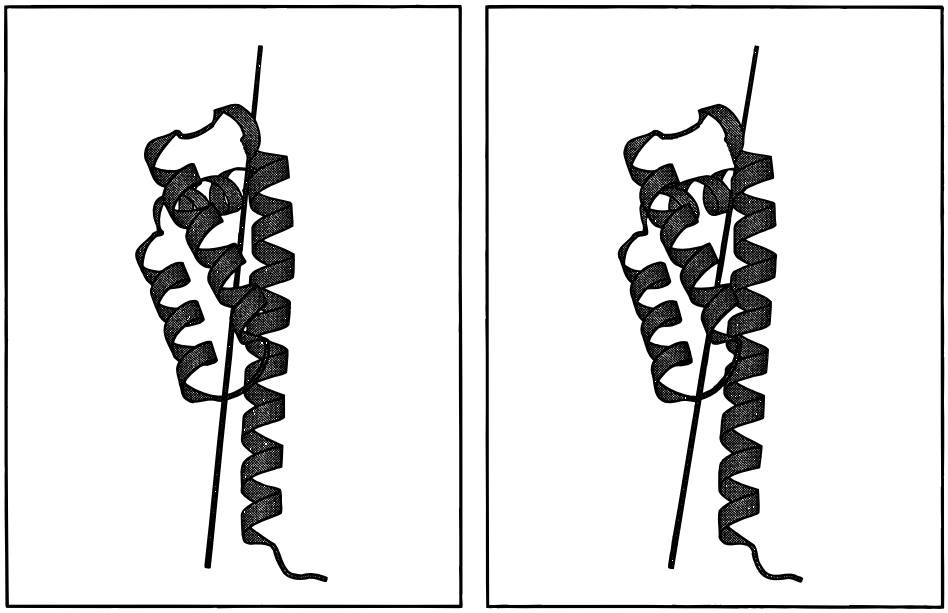

Fig. 5. The symmetrical diffusion axis of $DnaK_{518–638}$ aligned with the crystal structure of residues 529–607. The axis, pointing in the direction of $(\theta, \Phi) = (59°, 277°)$ (polar coordinates) in the coordinate frame of the crystal structure, was found by a grid search of the axis vector direction in the structure which best matches the set of angles (α) obtained from the dynamics analysis. The axis was drawn to pass through the geometrical center of residues 533–603 in the crystal structure.

protein. In particular, it seemed reasonable that this region might represent an intramolecular substrate for the peptide binding site. To test this possibility, we characterized the NMR spectrum of full-length DnaK. The resonances observed in the ^{1}H, ^{15}N spectrum of full-length DnaK are identical in position to the peaks assigned to the C-terminal mobile region in $DnaK_{518–638}$ (Fig. 7A,B). We confirmed that these peaks arise from the same residues by collecting two additional spectra: First, a sample of full-length DnaK having only the alanines labeled shows the correct number and position of resonances expected for the C-terminal mobile region (Fig. 7C). Second, the spectrum of a deletion mutant of DnaK ($DnaK_{1–605}$) in which the C-terminal 33 amino acids are removed completely lacks the peaks correlated with the C-terminal mobile region that are observed in the spectrum of full-length DnaK (Fig. 7D).

DnaK has a molecular weight of approximately 69 kDa and forms dimers and higher order oligomers under some conditions (Palleros et al., 1993; Schönfeld et al., 1995). NMR resonances are generally weak or unobservable for most of the residues in a molecule of this size due to the slow tumbling rate and correspondingly fast relaxation rates. However, flexible regions tumbling independently of the bulk of the molecule are often observable in the spectra of large proteins (for example, Gettins & Cunningham, 1986 and references therein; Landry et al., 1993). If the C-terminal mobile region of the C-terminal domain of DnaK is ordered in a stable interdomain contact in the full-length protein, it would tumble with the bulk of the molecule and its NMR resonances would be unobservable. If, on the other hand, it remains mobile in the context of the full-length protein, those resonances would remain observable in the spectrum.

Our result with full-length DnaK is consistent with a model in which the structured part of the C-terminal domain associates with the other domains of the molecule while the C-terminal tail region remains highly mobile. Interestingly, this pattern does not change upon the addition of ATP (not shown). Therefore, it appears that the mobile region is not involved in a stable interaction with the remainder of the protein in this context, regardless of the nucleotide state. This result, however, does not rule out the possibility of a transient interaction on a time scale that does not cause significant line broadening. Indeed, substantial biochemical evidence suggests that the mobile region modulates the affinity of peptide binding, possibly through a direct interaction with the peptide binding site (E.B. Bertelsen, P.R. Tsurada, F.W. Dahlquist, & G.C. Flynn, unpubl. obs.).

The resonances from the N-terminal disordered region (residues 518–531), which are intense in the spectrum of the fragment, are not present in the spectrum of the full-length protein. This region, therefore, appears to be structured and tumbling with the bulk of the molecule in the full-length protein, as expected based on its contacts to the peptide binding domain in the crystal structure (Zhu et al., 1996).

These data also address a model that has been proposed to account for the increased rate of peptide exchange of DnaK in the presence of ATP (Zhu et al., 1996). In this model, the interaction of the C-terminal domain with the peptide binding domain is disrupted in the ATP bound form by a melting of structure in the first helix. If the C-terminal domain simply loses its interdomain contacts and the melted linker region is substantially flexible in the ATP-bound state of DnaK, we might expect to observe the resonances from that domain in the NMR spectrum, since independent domains can be observed in the spectra of even very large modular proteins (McEvoy et al., 1997). The spectra of full-length DnaK suggest that the structured part of the C-terminal domain interacts with the other domains of the protein in both the ATP and ADP bound states, or the linker region remains fairly rigid even when it is released from the peptide binding site. This result is consistent with a more subtle conformational change, or a switching of in-

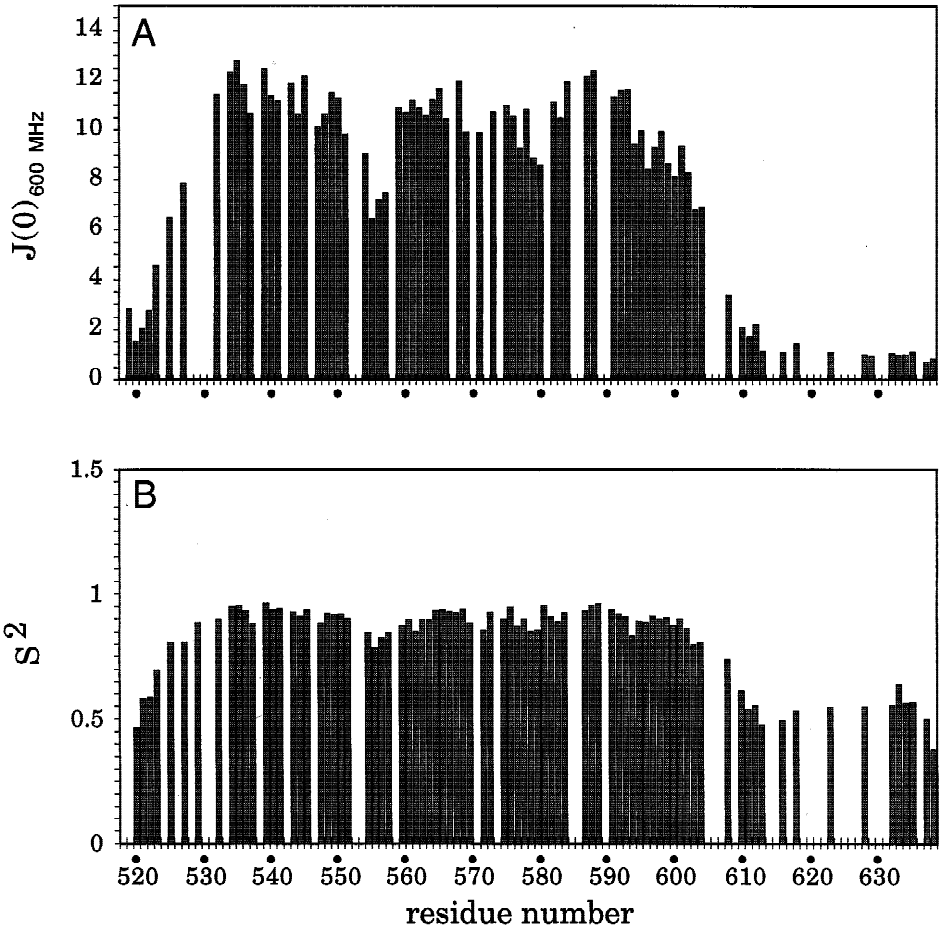

Fig. 6. Representative backbone dynamics. **A:** $J(0)$ at 600 MHz. **B:** S^2 plotted as a function of amino acid sequence.

teractions from the peptide binding domain to the ATPase domain in the ATP bound state.

Discussion

Structure of the C-terminal domain

$DnaK_{518–638}$ appears to contain two subdomains having distinct motional properties. The helical portion (residues 531–605) is stably folded and quite rigid, while the C-terminal 33 amino acids (residues 606–638) are highly mobile in solution. The secondary structural elements in solution for residues 531–605 are identical to those observed in the recent crystal structure of a larger fragment of DnaK containing this domain (Zhu et al., 1996). In addition, the results of our dynamics analysis support a similar three-dimensional fold for the molecule in solution and in the crystal. Overall, our results suggest that the global conformation of the C-terminal domain is independent of its contacts to the peptide binding domain, and support the idea that the C-terminal domain can act as a more or less rigid "lid" on the peptide binding domain. However, a high-resolution structure of the isolated C-terminal domain will be necessary to measure the extent of conformational change in this domain upon interaction with the peptide binding domain. Interestingly, there is a lack of protection from hydrogen exchange in the region proposed to play a role in hinge bending to promote the open conformation upon ATP binding, although dynamics measurements do not indicate an unusually high mobility in this region.

Using dynamics measurements to obtain global structural information

Although a large degree of rotational anisotropy poses some difficulties in the analysis of protein dynamics data, it can be used to distinguish differences in bond vector directions for dipolar-coupled spin pairs. This information helps us understand, for example, how several segments of the protein with known secondary structure are packed together. In the case of $DnaK_{518–638}$, the relative orientations of the amide bond vectors extracted from the dynamics data correlate fairly well with the crystal structure. Several large differences are seen that may be partially due to the uncertainties in the dynamics data, or perhaps indicate true differences in the bond vector directions between the solution structure and X-ray structure. Most of these differences were seen in the turn regions where the structure is relatively flexible and X-ray data contains high thermal factors (Zhu et al., 1996).

Our dynamics analysis differs from the methods used in many other studies (Bruschweiler et al., 1995; Tjandra et al., 1995) in that we extracted the dynamics parameters without reference to the crystal

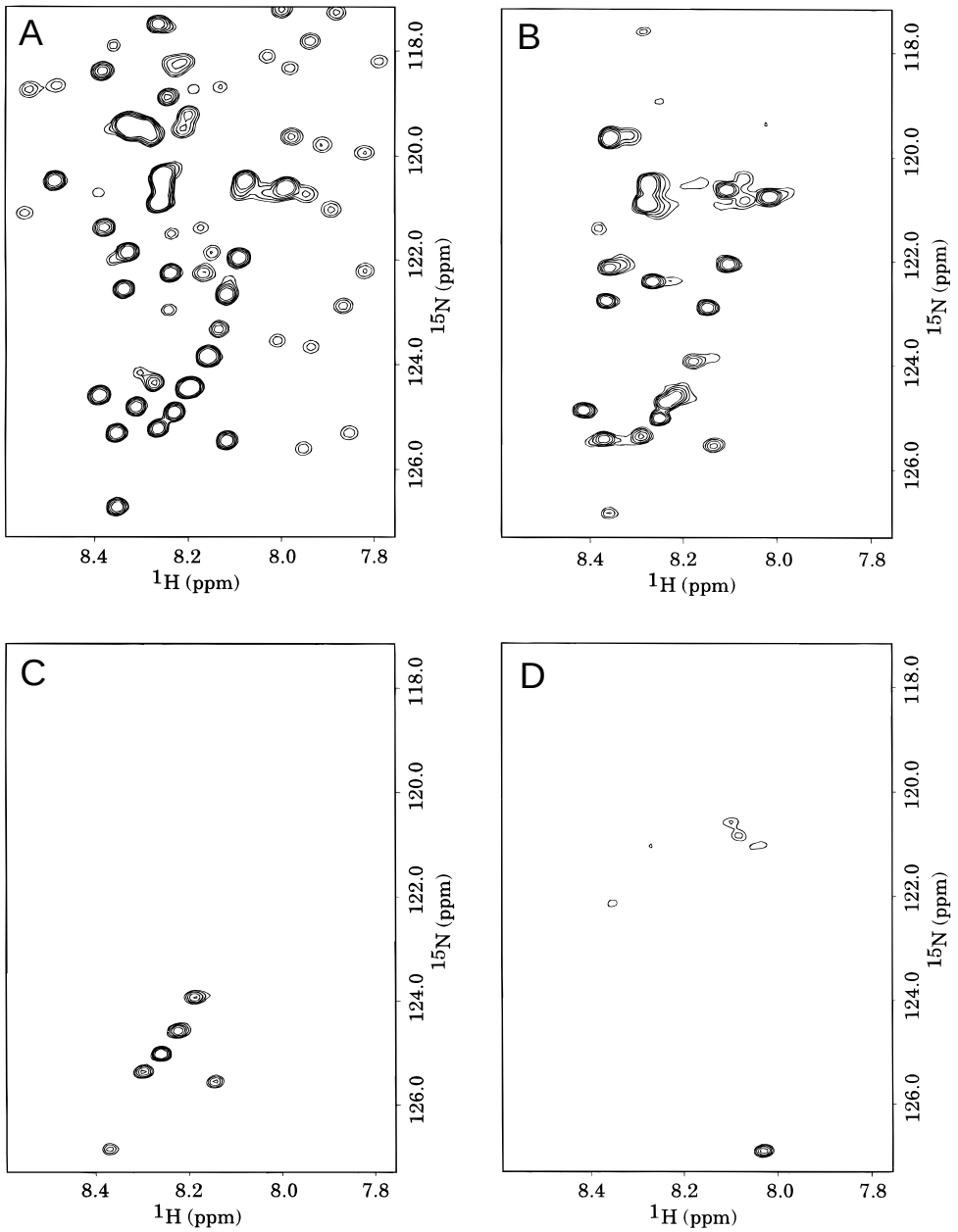

Fig. 7. Comparison of the ^{1}H, ^{15}N correlation spectra of DnaK$_{518–638}$ and full-length DnaK. A portion of the full spectrum (Fig. 2) containing the majority of the residues in the mobile region is shown. **A:** Uniformly ^{15}N-labeled DnaK$_{518–638}$. **B:** Uniformly ^{15}N-labeled full-length DnaK. **C:** ^{15}N-alanine labeled full-length DnaK. **D:** Uniformly ^{15}N-labeled DnaK$_{1–605}$. Specific peak assignments for **A** are shown in Figure 2.

structure. The extracted correlation times ($\tau_{\|}$ approximately 4.7 ns and $\tau_{\perp}$ approximately 13.4 ns), however, are similar to the ones that were found when the target function to be minimized is the difference between the angles from the dynamics data and those from the crystal coordinates ($\tau_{\|}$ approximately 5.3 ns and $\tau_{\perp}$ approximately 13.4 ns), although at the latter values the errors in the T_1/T_2 fits were slightly higher than when the T_1/T_2 ratios were directly fit. The extracted symmetric diffusion axes from the two methods are parallel within a few degrees. This consistency between different methods of data analysis demonstrates a degree of reliability in extracting the angles independent of the molecular coordinates. This approach, however, requires ^{15}N relaxation data collected at different fields or other independent measurements to provide a reliable fit, and is limited only to proteins with significant rotational anisotropy.

T_1/T_2 ratios have also been used to aid in structural refinement (Tjandra et al., 1997; Clore & Gronenborn, 1998). In addition, a T_1/T_2 ratio histogram method has been developed for evaluating anisotropic motion (Clore et al., 1998). This approach requires that the distribution of N-H bond vectors be approximately random with respect to one another, and seems poorly suited to our system since the orientation of the α-helices in the structured part of DnaK$_{518–638}$ results in a highly nonrandom distribution of N-H bond vectors.

In cases where the protein is globular, rotational anisotropy can be artificially enhanced by putting the protein in a liquid-crystalline medium, as shown by Tjandra and Bax (1997). In this study, instead of spin relaxation parameters, direction-dependent dipolar splittings due to a small degree of alignment of the molecule with the magnetic field were measured to obtain global structural information.

Conservation of structure

Primary sequence alignments of different Hsp70 family members have suggested structural similarities in the C-terminal domains. Although these regions have low sequence homology, many residues considered important in structural design are fairly well conserved (Zhu et al., 1996). Moreover, preliminary data on various Hsp70 family members are consistent with a conserved three-dimensional fold for the C-terminal domain. For example, mammalian BiP and bacterial DnaK generate a similar protease resistant C-terminal fragments from both full-length and N-terminally deleted proteins. Both of these fragments are thermally stable ($T_m >$ 65 °C) and highly helical (approximately 65% alpha helix) (not shown). In addition, the BiP fragment appears to possess a mobile region as shown here for the DnaK C-terminal domain (E.R.P. Zuiderweg, pers. comm.). Whether the overall three-dimensional folds of the C-terminal domains of BiP and DnaK are identical remains to be determined.

Role of the mobile region

In contrast to the apparently rigid structure of the helical portion of the molecule, the carboxy-terminal 33 residues are highly flexible. In the structural analysis by Zhu et al. (1996), residues 608–638 were removed, presumably because these residues interfered with crystallization. We have shown that these residues constitute a highly mobile subdomain of the protein and that this feature is conserved in the context of the full-length protein. Is this mobility a conserved feature of Hsp70 family members, and if so, what are the possible functions of this region?

Many Hsp70 family members contain a region of high G/P content near the extreme C-terminus (Boorstein et al., 1994). We have shown that the homologous region of DnaK, while relatively low in G/P content, is highly mobile in solution. Our results with DnaK, combined with the observation that these residues have a high propensity to be flexible (Creighton, 1993), suggest that this region is highly mobile in other Hsp70 family members as well. The mobility of this subdomain therefore appears to be a conserved feature of Hsp70 structure. Interestingly, other molecular chaperones also contain flexible regions. For example, DnaJ contains a conserved G/P-rich region, which has been shown to be mobile in solution (Szyperski et al., 1994; Pellecchia et al., 1996). This flexible region of DnaJ appears to mediate the interaction between DnaJ and DnaK by binding to the peptide binding site of DnaK (Wall et al., 1995; Karzai & McMacken, 1996). Likewise, GroES (the *E. coli* Hsp10) contains a flexible loop that becomes immobilized upon interaction with the *E. coli* Hsp60, GroEL (Landry et al., 1993, 1996). In addition, the mammalian Hsc70 regulator, Hip, contains an Hsp70-like G/P-rich region (Höhfeld et al., 1995). It remains to be seen whether these flexible regions have similar or divergent roles in the functions of molecular chaperones.

The motif EEVD appears at the extreme C-terminus of many Hsp70s (Boorstein et al., 1994; Freeman et al., 1995). In human Hsp70, this motif appears to be involved in peptide binding, ATPase activity, and interactions with the human DnaJ homolog, HDJ1 (Freeman et al., 1995). DnaK contains the motif EEV near to the C-terminus (Fig. 3). Although we have no data addressing a functional role of this motif in DnaK, it is interesting to speculate that a general feature of Hsp70 architecture is to place an important motif at the end of a flexible linker of varying length. This motif and possibly the entire mobile region may become structured during an interaction with a protein cofactor such as DnaJ or its homologs. It is also possible that this flexible region is important for the separation of the ER retention signal in BiP (KDEL) from the remainder of the molecule.

The structuring of a mobile region of a molecular chaperone in a protein–protein interaction may have important thermodynamic consequences (Landry et al., 1996; Pellecchia et al., 1996). Unstructured domains can act to increase the rate of complex formation (Pontius, 1993). Alternatively, the entropically favorable flexibility attained upon release may prevent the interaction from being too tight. This switching between structure and flexibility may provide a layer of regulation for the energetics of the interaction. Indeed, if the mobile region is involved in making contacts to the peptide binding site, as is the case with DnaJ, it may provide the chaperone with the ability to fine-tune the energetics of peptide binding and release, preventing peptide interactions that are too tight or stimulating the exchange of peptides between molecular chaperones of different classes.

Materials and methods

Plasmid construction

Plasmid pDnaK$_{401–638}$ was constructed by PCR amplification using the plasmid pKJ (Gragerov et al., 1992) as the template. Primers were designed to introduce BamHI and HindIII restriction sites at the 5′ and 3′ ends of the amplified product, respectively. The PCR fragments were digested with the appropriate restriction endonucleases and ligated into the plasmid pQE30 (Qiagen). The resulting plasmid expresses amino acids 401–638 of DnaK fused to the N-terminal sequence MRGHHHHHHGSIEGR. The plasmid pDnaK(ΔJ), which expresses full-length DnaK, was constructed by deleting a StuI–SmaI fragment containing most of the coding region of DnaJ from pKJ.

NMR sample preparation

^{15}N-labeled and ^{15}N/^{13}C-labeled samples of the C-terminal domain of DnaK (residues 518–638) were prepared by trypsin digestion of a larger C-terminal fragment of DnaK as follows: *E. coli* (XL-1 Blue) harboring the plasmid pDnaK$_{401–638}$ were grown to mid-log stage in the appropriate minimal medium (Muchmore et al., 1989). DnaK$_{401–637}$ expression was induced by the addition of 1 mM IPTG and overnight shaking at 37 °C. Cells were harvested by centrifugation, resuspended in buffer A (50 mM Tris·HCl, 200 mM NaCl, pH 7.5), and lysed in a french pressure cell. Extracts were clarified by centrifugation at 40 K × *g* for 40 min, and the protein was purified on Ni^{++}/NTA agarose (Qiagen) according to the manufacturer's suggestions. Fractions from the Ni^{++}/NTA column (in buffer A plus 200 mM imidazole) were combined and subjected to trypsin digestion by adding 1:1000 (w:w) trypsin: DnaK and incubating at 37 °C for 45–60 min. The reaction was

quenched by addition of PMSF to 1 mM and freezing in liquid N_2. Aliquots were then thawed and diluted 1/10 with buffer B (50mM Tris·HCl, pH 7.2) and applied to either MonoQ or Q Sepharose Fast Flow (Pharmacia, Uppsala, Sweden) columns. The column was washed with buffer B, then eluted with an NaCl gradient (50–350 mM in buffer B). Peak fractions were combined, supplemented with 1 mM PMSF, and dialyzed against 50 mM sodium phosphate, pH 7.0/100 mM NaCl. Purity was confirmed by reverse-phase HPLC analysis. Prior to NMR analysis, protein was concentrated to approximately 1 mM. The buffer was then exchanged to NMR buffer (100 mM sodium phosphate, 100 mM NaCl, 0.01% sodium azide, 10% ^2H_2O, pH 6.1) either by dialysis or by spinning through Sephadex G-25 resin.

Full-length DnaK was prepared by purification on ATP-agarose essentially as described (Mensa-Wilmot et al., 1989). Briefly, DnaK was expressed in the appropriate medium for specific or uniform ^{15}N-labeling (Muchmore et al., 1989). Clarified cell extracts (prepared as described above) in DnaK buffer (25 mM Tris·HCl, pH 7.0, 35 mM KCl, 10 mM $MgCl_2$) were applied to a 12 mL ATP agarose (Sigma A2767) column pre-equilibrated with the same buffer. The column was washed with DnaK buffer and eluted with DnaK buffer containing 3 mM ATP. Peak fractions were pooled, diluted 10-fold with 50 mM Tris, pH 7.5, and applied to a Q Sepharose Fast Flow (Pharmacia) column. Protein was eluted with a 0–350 mM gradient of NaCl in Tris buffer. Peak fractions were pooled, dialyzed against DnaK buffer, and concentrated to approximately 0.15 mM.

NMR spectroscopy

NMR spectra were recorded at 25 °C and referenced externally to sodium 2,2-dimethyl-2-silapentane-5-sulfonate (DSS). Lawrence McIntosh (University of British Columbia) kindly collected the HNCACB and CBCA(CO)NH spectra on a Varian Unity-plus 500 MHz spectrometer. The remainder of the data sets were collected on either a Varian Inova 600 MHz spectrometer (for triple resonance experiments) or a GE Omega 500 MHz spectrometer (for double resonance experiments). In addition, a complete backbone dynamics data set was obtained on a Varian Unity-plus 750 MHz spectrometer. The Varian spectrometers are equipped with triple-resonance, pulsed-field gradient probes.

The following data sets were acquired for sequential resonance assignments and secondary structure analysis: Sequential resonance assignments via scalar couplings for the C_α and C_β carbons were obtained from the sensitivity enhanced HNCACB (Wittekind & Mueller, 1993; Muhandiram & Kay, 1994) and CBCA(CO)NH (Grzesiek & Bax, 1992; Muhandiram & Kay, 1994) experiments. Side-chain carbon and proton resonance assignments were obtained from C(CO)NH and H(CCO)NH experiments (Grzesiek et al., 1993; Grzesiek & Bax, 1993), respectively. Assignments for carbonyl carbons were obtained from the sensitivity enhanced HNCO experiment (Kay et al., 1990, 1994). Sequential NOEs were obtained from a 3D, ^1H, ^{15}N NOESY-HSMQC spectrum (Marion et al., 1989; Zuiderweg & Fesik, 1989) recorded at 500 MHz with a mixing time of 100 ms. Backbone dihedral angle Φ estimates were obtained by measuring the coupling constants $^3J_{HN\alpha}$ from a series of J-modulated ^1H, ^{15}N COSY spectra (Billeter et al., 1992). Residues protected from hydrogen exchange were identified in a series of HSMQC spectra (Zuiderweg, 1990) collected immediately after exchanging a sample into ^2H_2O buffer using a G-25 Sephadex spin column. It was estimated that residues still present in the first spectrum following exchange into ^2H_2O were protected at least 10^3 relative to a random coil peptide (Bai et al., 1993).

Full-length DnaK was characterized by collecting ^1H, ^{15}N correlation spectra at 600 MHz. To test the effect of the nucleotide state on the spectrum, ATP was added to a concentration of 1 mM and a 75 min spectrum was acquired immediately. We estimated that complete hydrolysis of ATP would require at least 130 min, based on a turnover number of 0.05 min^{-1}. Because conversion of ATP to ADP is rate-limiting under these conditions (McCarty et al., 1995), we expect the resulting spectrum to represent the ATP-bound conformation.

^{15}N relaxation

Two-dimensional (2D) inverse-detection techniques were used to measure ^{15}N longitudinal (T_1) and transverse (T_2) relaxation times, and the heteronuclear $^{15}N\{^1H\}$ NOE (Kay et al., 1989; Clore et al., 1990; Barbato et al., 1992; Farrow et al., 1994) for $DnaK_{518–638}$. T_1 and T_2 values were extracted from data collected at proton frequencies of 500, 600, and 750 MHz; $^{15}N\{^1H\}$ NOEs were measured at 600 and 750 MHz. Overlapped or extremely weak peaks were excluded from analysis. The T_1/T_2 ratios at the three fields were fit simultaneously using a model for isotropic motion, axially symmetric anisotropic motion, or general anisotropic motion to extract parameters describing overall motion of the molecule and the angles related to the amide bond vector directions. The best model obtained was then used to simultaneously fit the dynamics observables (T_1, T_2, and NOE) at the three fields to extract parameters describing internal motions.

Under the condition that internal motion is much faster than overall motion, the spectral density for an isotropic motion is related to a single overall correlation time (τ_m) and an order parameter (S^2) by the following equation (Lipari & Szabo, 1982):

$$J(\omega) = \frac{S^2\tau_m}{[1 + (\omega\tau_m)^2]}. \quad (1)$$

In the anisotropic model for molecules with an axially symmetric shape, the spectral density is given by the equation (Woessner, 1962; Tjandra et al., 1995):

$$J(\omega) = S^2\left\{\frac{A_1\tau_1}{[1 + (\tau_1\omega)^2]} + \frac{A_2\tau_2}{[1 + (\tau_2\omega)^2]} + \frac{A_3\tau_3}{[1 + (\tau_3\omega)^2]}\right\} \quad (2)$$

with $A_1 = (1.5\cos^2\alpha - 0.5)^2$, $A_2 = 3\sin^2\alpha\cos^2\alpha$, and $A_3 = 0.75\sin^4\alpha$, where α is the angle between the amide bond vector and the axis of symmetrical rotational diffusion. The time constants are related to the two diffusion constants $D_\perp$ ($=D_x=D_y$) and $D_\perp(=D_z)$ about the principal diffusion axes by $\tau_1 = 1/(6D_\perp)$, $\tau_2 = 1/(D_\parallel + 5D_\perp)$ and $\tau_3 = 1/(4D_\parallel + 2D_\perp)$.

Extension of the axially symmetrical diffusion model to a general diffusion model for an arbitrarily shaped molecule requires the introduction of a total of six global parameters. These include three independent correlation times around the three principal rotational diffusion axes and three angles defining the orientations of these axes (Woessner, 1962; Tjandra et al., 1995).

An initial estimate of S^2 by fitting T_1/T_2 using Equation 1 indicated that residues 16–86 (533–603) form a rigid structure

($S^2 > 0.8$) and the N- and C-terminal regions are flexible ($S^2 < 0.6$). The exchange effects to the T_2 values were estimated from the differences between the spectral density terms $J(0)$ measured at 600 and 750 MHz since exchange broadening would shorten T_2 and cause a strong field dependence in $J(0)$ (Farrow et al., 1997). The $J(0)$ values were extracted analytically from T_1, T_2, and NOE values along with $J(\omega_N)$ and $J(\omega_H)$ under the approximation $J(\omega_H) \approx J(\omega_H + \omega_N) \approx J(\omega_H - \omega_N)$ (Farrow et al., 1995). The pairwise differences between the $J(0)$ values from the data sets at the two fields are less than 8%, indicating no significant exchange contributions to T_2 values for most of the residues. Three residues (567, 571, and 577) exhibit large differences (more than twice the standard deviation) and were excluded from the extraction of overall correlation time(s). Therefore, the region containing residues 533–603, except for the residues excluded as indicated above, were used to evaluate the parameters for the overall motion of the rigid structure. This was done by minimizing the total, fractional differences between experimental T_1/T_2 and calculated T_1/T_2 values:

$$E_1 = \Sigma_{i,500,600,750\ \mathrm{MHz}} \left[\frac{(T_{1,cal}/T_{2,cal} - T_{1,exp}/T_{2,exp})^2}{(T_{1,exp}/T_{2,exp})^2} \right] \quad (3)$$

where the sum is taken over all selected residues at the three fields. In the axially symmetric diffusion model (Equation 2), the minimization of E_1 was done by a grid search in the two diffusion constants $D_\perp$ and $D_\parallel$ (or the corresponding rotational correlation times, $\tau_\perp = 1/(6D_\perp)$ and $\tau_\parallel = 1/(6D_\parallel)$) and by Powell's method in the set of angles α. Uncertainties in the extracted correlation times were estimated using the bootstrap method of Monte Carlo simulation (Press et al., 1992). During the simulation, approximately 37% randomly selected data points were replaced by synthesized data, which contain random noise with Gaussian distributions and standard deviations of 5 and 10% of the experimental T_1 and T_2 values, respectively. These uncertainty ranges were set to be larger than the values (<3% for T_1, <5% for T_2, and <8% for T_1/T_2) estimated from the noise levels and duplicated data sets at 600 MHz to include additional potential uncertainties.

Internal motion parameters S^2 and τ_e were extracted for each residue after the parameters for overall motion were determined. In the axially symmetric model, internal motions were included in the following definition of the spectral density (Tjandra et al., 1995):

$$J(\omega) = S^2 \left\{ \frac{A_1\tau_1}{[1+(\tau_1\omega)^2]} + \frac{A_2\tau_2}{[1+(\tau_2\omega)^2]} + \frac{A_3\tau_3}{[1+(\tau_3\omega)^2]} \right\} + \frac{(1-S^2)\tau}{[1+(\tau\omega)^2]} \quad (4)$$

where $\tau^{-1} = 6D + \tau_e{}^{-1}$, with $D = (D_x + D_y + D_z)/3$. The following function was minimized to extract S^2, τ_e, and the angle α for each residue while τ_1, τ_2, and τ_3 were fixed at the best values obtained:

$$E_2 = \Sigma_{i,500,600,750\ \mathrm{MHz}} \left\{ \left[\frac{(T_{1,cal} - T_{1,exp})}{T_{1,exp}} \right]^2 + \left[\frac{(T_{2,cal} - T_{2,exp})^2}{T_{2,exp}} \right]^2 \right\} + \Sigma_{i,600,750\ \mathrm{MHz}} \left[\frac{(NOE_{cal} - NOE_{exp})}{NOE_{exp}} \right]^2. \quad (5)$$

Supplementary material in Electronic Appendix

Table 1 contains chemical shift values for backbone ^{15}N-H, ^{15}N, Cα, Cβ, and carbonyl carbon resonances. Table 2 contains values for the dynamics parameters T_1, T_2, and ^{15}N{^{1}H} NOE.

Acknowledgments

We thank Fred Hughson and Erik Zuiderweg for sharing data, and Megan McEvoy for helpful discussions. Lawrence McIntosh kindly collected some of the NMR data and Logan Donaldson provided useful Felix macros. This work was supported by NIH grants to F.W.D. and E.B.B. was the recipient of an NIH National Research Service Award Pre-Doctoral Training Grant. NMR data collection at 750 MHz was supported by the U.S. Department of Energy under contract DE-AC06-76RLO-1830.

References

Bai Y, Milne JS, Mayne L, Englander SW. 1993. Primary structure effects on peptide group hydrogen exchange. *Proteins 17*:75–86.

Barbato G, Ikura M, Kay LE, Pastor RW, Bax A. 1992. Backbone dynamics of calmodulin studied by ^{15}N relaxation using inverse detected two-dimensional NMR spectroscopy: The central helix is flexible. *Biochemistry 31*:5269–5278.

Billeter M, Neri D, Otting G, Qian YQ, Wüthrich K. 1992. Precise vicinal coupling constants $^3J_{HN\alpha}$ in proteins from nonlinear fits of J-modulated [^{15}N,^{1}H]-COSY experiments. *J Biomol NMR 2*:257–274.

Bolliger L, Deloche O, Glick BS, Georgopoulos C, Jeno P, Kronidou N, Horst M, Morishima N, Schatz G. 1994. A mitochondrial homolog of bacterial GrpE interacts with mitochondrial Hsp70 and is essential for viability. *EMBO J 13*:1998–2006.

Boorstein WR, Ziegelhoffer T, Craig EA. 1994. Molecular evolution of the HSP70 multigene family. *J Mol Evol 38*:1–17.

Bruschweiler R, Liao X, Wright PE. 1995. Long-range motional restrictions in a multidomain zinc-finger protein from anisotropic tumbling. *Science 268*:886–889.

Buchberger A, Theyssen H, Schroder H, McCarty JS, Virgallita G, Milkereit P, Reinstein J, Bukau B. 1995. Nucleotide-induced conformational changes in the ATPase and substrate binding domains of the DnaK chaperone provide evidence for interdomain communication. *J Biol Chem 270*:16903–16910.

Bukau B, Walker GC. 1990. Mutations altering heat shock specific subunit of RNA polymerase suppress major cellular defects of *E. coli* mutants lacking the DnaK chaperone. *EMBO J 9*:4027–4036.

Caplan AJ, Cyr DM, Douglas MG. 1993. Eukaryotic homologues of *Escherichia coli* DnaJ: A diverse protein family that functions with Hsp70 stress proteins. *Mol Biol Cell 4*:555–563.

Chappell TG, Konforti BB, Schmid SL, Rothman JE. 1987. The ATPase core of a clathrin uncoating protein. *J Biol Chem 262*:746–751.

Clore MG, Driscoll PC, Wingfield PT, Gronenborn AM. 1990. Analysis of the backbone dynamics of interleukin-1 beta using two-dimensional inverse detected heteronuclear ^{15}N-^{1}H NMR spectroscopy. *Biochemistry 29*:7387–7401.

Clore MG, Gronenborn AM. 1998. New methods of structure refinement for macromolecular structure determination by NMR. *Proc Natl Acad Sci USA 95*:5891–5898.

Clore MG, Gronenborn AM, Szabo A, Tjandra N. 1998. Determining the magnitude of the fully asymmetric diffusion tensor from heteronuclear relaxation data in the absence of structural information. *J Am Chem Soc 120*:4889–4890.

Creighton TE. 1993. *Proteins: Structures and molecular properties*, 2nd ed. New York: W.H. Freeman and Company.

Farrow NA, Muhandiram R, Singer AU, Pascal SM, Kay CM, Gish G, Shoelson SE, Pawson T, Forman-Kay JD, Kay LE. 1994. Backbone dynamics of a free and phosphopeptide-complexed Src homology 2 domain studied by ^{15}N NMR relaxation. *Biochemistry 33*:5984–6003.

Farrow NA, Zhang O, Forman-Kay JD, Kay LE. 1995. Comparison of the backbone dynamics of a folded and an unfolded SH3 domain existing in equilibrium in aqueous buffer. *Biochemistry 34*:868–878.

Farrow NA, Zhang O, Forman-Kay JD, Kay LE. 1997. Characterization of the backbone dynamics of folded and denatured states of an SH3 domain. *Biochemistry 36*:2390–2402.

Flaherty KM, DeLuca-Flaherty C, McKay DB. 1990. Three-dimensional structure of the ATPase fragment of a 70 K heat-shock cognate protein. *Nature 346*:623–628.

Freeman BC, Myers MP, Schumacher R, Morimoto RI. 1995. Identification of a regulatory motif in Hsp70 that affects ATPase activity, substrate binding and interaction with HDJ-1. *EMBO J 14*:2281–2292.

Georgopoulos C, Liberek K, Zylicz M, Ang D. 1994. Properties of the heat shock proteins of *Escherichia coli* and the autoregulation of the heat shock response. In: Morimoto RI, Tissières A, Georgopoulos C, eds. *The biology of heat shock proteins and molecular chaperones.* Plainview, NY: Cold Spring Harbor Laboratory Press. pp 209–249.

Gething M-J, Sambrook J. 1992. Protein folding in the cell. *Nature 355*:33–45.

Gettins P, Cunningham LW. 1986. Identification of ^{1}H resonances from the bait region of human a_2-macroglobulin and effects of proteases and methylamine. *Biochemistry 25*:5011–5017.

Gragerov A, Nudler E, Komissarova N, Gaitanaris GA, Gottesman ME, Nikiforov V. 1992. Cooperation of GroEL/GroES and DnaK/DnaJ heat shock proteins in preventing protein misfolding in *Escherichia coli*. *Proc Natl Acad Sci USA 89*:10341–10344.

Grzesiek S, Anglister J, Bax A. 1993. Correlation of backbone amide and aliphatic side-chain resonances in ^{13}C/^{15}N-enriched proteins by isotropic mixing of ^{13}C magnetization. *J Magn Reson, Ser B 101*:114–119.

Grzesiek S, Bax A. 1992. Correlating backbone amide and side chain resonances in larger proteins by multiple relayed triple resonance NMR. *J Am Chem Soc 114*:6291–6293.

Grzesiek S, Bax A. 1993. The importance of not saturating H_2O in protein NMR. Application to sensitivity enhancement and NOE measurements. *J Am Chem Soc 115*:12593–12594.

Ha J-H, McKay DB. 1994. ATPase kinetics of recombinant bovine 70 kDa heat shock cognate protein and its amino-terminal ATPase domain. *Biochemistry 33*:14625–14635.

Harrison CJ, Hayer-Hartl M, Di Liberto M, Hartl F-U, Kuriyan J. 1997. Crystal structure of the nucleotide exchange factor GrpE bound to the ATPase domain of the molecular chaperone DnaK. *Science 276*:431–435.

Hendrick JP, Hartl F-U. 1995. The role of molecular chaperones in protein folding. *FASEB J 9*:1559–1569.

Höhfeld J, Minami Y, Hartl F-U. 1995. Hip, a novel cochaperone involved in the eukaryotic Hsc70/Hsp40 reaction cycle. *Cell 83*:589–598.

Karzai AW, McMacken R. 1996. A bipartite signaling mechanism involved in DnaJ-mediated activation of the *Escherichia coli* DnaK protein. *J Biol Chem 271*:11236–11246.

Kassenbrock CK, Kelly RB. 1989. Interaction of heavy chain binding protein (BiP/GRP78) with adenine nucleotides. *EMBO J 8*:1461–1467.

Kay LE, Ikura M, Tschudin R, Bax A. 1990. Three-dimensional triple-resonance NMR spectroscopy of isotopically enriched proteins. *J Magn Reson 89*:496–514.

Kay LE, Torchia DA, Bax A. 1989. Backbone dynamics of proteins as studied by ^{15}N inverse detected heteronuclear NMR spectroscopy: Application to staphylococcal nuclease. *Biochemistry 28*:8972–8979.

Kay LE, Xu GY, Yamazaki T. 1994. Enhanced-sensitivity triple-resonance spectroscopy with minimal H_2O saturation. *J Magn Reson, Ser A 109*:129–133.

Landry SJ, Taher A, Georgopoulos C, van der Vies SM. 1996. Interplay of structure and disorder in cochaperonin mobile loops. *Proc Natl Acad Sci USA 93*:11622–11627.

Landry SJ, Zeilstra-Ryalls J, Fayet O, Georgopoulos C, Gierasch LM. 1993. Characterization of a functionally important mobile domain of GroES. *Nature 364*:255–258.

Liberek K, Marszalek J, Ang D, Georgopoulos C, Zylicz M. 1991. *Escherichia coli* DnaJ and GrpE heat shock proteins jointly stimulate ATPase activity of DnaK. *Proc Natl Acad Sci USA 88*:2874–2878.

Lipari G, Szabo A. 1982. Model-free approach to the interpretation of nuclear magnetic resonance relaxation in macromolecules. 1. Theory and range of validity. 2. Analysis of experimental results. *J Am Chem Soc 104*:4546–4570.

Marion D, Kay LE, Sparks SW, Torchia DA, Bax A. 1989. Three-dimensional heteronuclear NMR of ^{15}N-labeled proteins. *J Am Chem Soc 111*:1515–1517.

McCarty JS, Buchberger A, Reinstein J, Bukau B. 1995. The role of ATP in the functional cycle of the DnaK chaperone system. *J Mol Biol 249*:126–137.

McEvoy MM, De La Cruz AFA, Dahlquist FW. 1997. Large modular proteins by NMR. *Nat Struct Biol 4*:9.

Mensa-Wilmot K, Seaby R, Wold MC, Gomes B, McMacken R. 1989. Reconstitution of a nine-protein system that initiates bacteriophage lambda replication. *J Biol Chem 264*:2853–2861.

Morshauser RC, Wang H, Flynn GC, Zuiderweg ERP. 1995. The peptide-binding domain of the chaperone-protein Hsc70 has an unusual secondary structure topology. *Biochemistry 34*:6261–6266.

Muchmore DC, McIntosh LP, Russell CB, Anderson ED, Dahlquist FW. 1989. Expression and nitrogen-15 labeling of proteins for proton and nitrogen-15 nuclear magnetic resonance. *Methods Enzymol 177*:44–73.

Muhandiram DR, Kay LE. 1994. Gradient-enhanced triple-resonance three-dimensional NMR experiments with improved sensitivity. *J Magn Reson Ser B 103*:203–216.

Palleros DR, Ried KL, Shi L, Fink AL. 1993. DnaK ATPase revisited. *FEBS Lett 336*:121–128.

Pellecchia M, Szyperski T, Wall D, Georgopoulos C, Wüthrich K. 1996. NMR structure of the J-domain and the Gly/Phe-rich region of the *Escherichia coli* DnaJ chaperone. *J Mol Biol 260*:236–250.

Pontius BW. 1993. Close encounters: Why unstructured, polymeric domains can increase rates of specific macromolecular association. *Trends Biochem Sci 18*:181–186.

Press WH, Teukolsky SA, Vetterling WT, Hannery BP. 1992. *Numerical recipes*. Cambridge, UK: Cambridge University Press.

Rüdiger S, Buchberger A, Bukau B. 1997. Interaction of Hsp70 chaperones with substrates. *Nat Struct Biol 4*:342–349.

Russell R, Jordan R, McMacken R. 1998. Kinetic characterization of the ATPase cycle of the DnaK molecular chaperone. *Biochemistry 37*:596–607.

Schönfeld H-J, Schmidt D, Schröeder H, Bukau B. 1995. The DnaK chaperone system of *Escherichia coli*: Quaternary structures and interactions of the DnaK and GrpE components. *J Biol Chem 270*:2183–2189.

Silver PA, Way JC. 1993. Eukaryotic DnaJ homologs and the specificity of Hsp70 activity. *Cell 74*:5–6.

Stuart RA, Cyr DM, Craig EA, Neupert W. 1994. Mitochondrial molecular chaperones: Their role in protein translocation. *Trends Biochem Sci 19*: 87–92.

Szyperski T, Pellecchia M, Wall D, Georgopoulos C, Wüthrich K. 1994. NMR structure determination of the *Escherichia coli* DnaJ molecular chaperone: Secondary structure and backbone fold of the N-terminal region (residues 2–108) containing the highly conserved J domain. *Proc Natl Acad Sci USA 91*:11343–11347.

Tjandra N, Bax A. 1997. Direct measurement of distances and angles in biomolecules by NMR in a dilute liquid crystalline medium. *Science 278*:1111–1114.

Tjandra N, Feller SE, Pastor RW, Bax A. 1995. Rotational diffusion anisotropy of human ubiquitin from ^{15}N NMR relaxation. *J Am Chem Soc 117*:12562–12566.

Tjandra N, Garrett DS, Gronenborn AM, Bax A, Clore GM. 1997. Defining long range order in NMR structure determination from the dependence of heteronuclear relaxation times on rotational diffusion anisotropy. *Nat Struct Biol 4*:443–449.

Tsai M-Y, Wang C. 1994. Uncoupling of peptide-stimulated ATPase and clathrin-uncoating activity in deletion mutant of Hsc70. *J Biol Chem 269*:5958–5962.

Wall D, Zylicz M, Georgopoulos C. 1995. The conserved G/F motif of the DnaJ chaperone is necessary for the activation of the substrate binding properties of the DnaK chaperone. *J Biol Chem 270*:2139–2144.

Wang H, Kurochkin AV, Pang Y, Hu W, Flynn GC, Zuiderweg ER. 1998. NMR solution structure of the 21 kDa chaperone protein DnaK substrate binding domain: A preview of chaperone-protein interaction. *Biochemistry 37*:7929–7940.

Wang T-F, Chang J-H, Wang C. 1993. Identification of the peptide binding domain of Hsc70. *J Biol Chem 268*:26049–26051.

Wawrzynow A, Zylicz M. 1995. Divergent effects of ATP on the binding of the DnaK and DnaJ chaperones to each other, or to their various native and denatured protein substrates. *J Biol Chem 270*:19300–19306.

Wishart DS, Sykes BD. 1994. Chemical shifts as a tool for structure determination. *Methods Enzymol 239*:363–392.

Wittekind M, Mueller L. 1993. HNCACB, a high-sensitivity 3D NMR experiment to correlate amide-proton and nitrogen resonances with the alpha- and beta-carbon resonances in proteins. *J Magn Reson Ser B 101*:201–205.

Woessner DE. 1962. Nuclear spin relaxation in ellipsoids undergoing rotational Brownian motion. *J Chem Phys 37*:647–654.

Zhu X, Zhao X, Burkholder WF, Gragerov A, Ogata CM, Gottesman ME, Hendrickson WA. 1996. Structural analysis of substrate binding by the molecular chaperone DnaK. *Science 272*:1606–1614.

Zuiderweg ERP. 1990. A proton-detected heteronuclear chemical-shift correlation experiment with improved resolution and sensitivity. *J Magn Reson 86*:346–357.

Zuiderweg ERP, Fesik SW. 1989. Heteronuclear three-dimensional NMR spectroscopy of the inflammatory protein C5A. *Biochemistry 28*:2387–2391.